Mechanical Systems and Signal Processing 147 (2021) 107128

Contents lists available at ScienceDirect

Mechanical Systems and Signal Processing

journal homepage: www.elsevier.com/locate/ymssp

Path-following control of Mecanum-wheels omnidirectional mobile robots using nonsingular terminal sliding mode

Zhe Sun [a,*], Hao Xie [b], Jinchuan Zheng [b], Zhihong Man [b], Defeng He [a]

[a] College of Information Engineering, Zhejiang University of Technology, Hangzhou, China
[b] School of Software and Electrical Engineering, Swinburne University of Technology, Melbourne, Australia

ARTICLE INFO

Article history:
Received 18 February 2020
Received in revised form 15 May 2020
Accepted 5 July 2020
Available online 18 July 2020

Keywords:
Mobile robot
Path following
Mecanum wheel
Nonsingular terminal sliding mode (NTSM)

ABSTRACT

Due to the superior mobility and maneuverability to move toward any position and attain any orientation simultaneously, Mecanum-wheels omnidirectional mobile robot (MWOMR) is playing a significant role in autonomous transportation and service. This paper proposes a robust nonsingular terminal sliding mode (NTSM) control scheme for the path-following problem of an MWOMR. First, a plant model is identified as a second-order state-space equation with four inputs and three outputs to describe the MWOMR's path-tracking kinematics and dynamics. Afterwards, a multi–input–multi–output NTSM controller is designed for the MWOMR, and the stability of the NTSM control system is verified by means of Lyapunov function. In addition, the setting guideline of control parameters is elaborated in detail, and a Runge–Kutta formula-based dead-reckoning algorithm is employed to calculate the position and yaw angle information of the robot in real time. Lastly, experiments are carried out to test the control performance in the scenarios of lateral movement and circular movement with initial offset. Experimental results demonstrate that the presented NTSM control strategy owns evident superiority in terms of higher tracking accuracy and stronger robustness against different movements in comparison with a conventional sliding mode (CSM) controller.

1. Introduction

Mobile robots are widely utilized to transport products in factories and warehouses or provide services in families autonomously [1–5]. The comprehensive application of mobile robots is able to replace human labor and increase working efficiency to a large extent. Conventional mobile robot (CMR) is normally with rubber wheels, such as two-wheels differential-steering mobile robots [6]. An obvious drawback of a CMR is that it cannot move in any direction instantaneously but requires a turnabout or a switchback [7]. To overcome this shortcoming, omnidirectional mobile robot (OMR) is developed, which is normally with several specially designed wheels such that it can move sideways to obtain higher maneuverability [8,9].

Compared with CMR, OMR possesses superior agile capability to move in any direction and toward any position without reorientation. Due to its remarkable benefits, OMR has attracted considerable attention from researchers and engineers. One type of OMR is with spherical wheels [10,11]. Specifically, a novel omnidirectional spherical robot is designed, where a

* Corresponding author.
E-mail address: sunzhe726@zjut.edu.cn (Z. Sun).

https://doi.org/10.1016/j.ymssp.2020.107128
0888-3270/

driven ball is installed inside a spherical shell and driven by two orthogonally-mounted rollers to achieve omnidirectional mobility [12]. Another typical type is the three-wheels OMR, which normally consists of a rounded body and three wheels forming a triangular shape in a top view [13,14]. Recently, some newly developed OMRs have attracted attention from academy and industry. For instance, a snake-like robot using screw-drive units connected by active joints is proposed, which can achieve the omnidirectional mobility by the combination of screws' angular velocities [15]. In [16], a novel slidable-wheels OMR is designed, which has three wheels connected to the robot body by passive sliding joints such that both omnidirectional mobility and structural reliability can be guaranteed. Mecanum-wheels omnidirectional mobile robot (MWOMR) is another typical and innovative kind of OMR, whose Mecanum wheels are designed with passive rollers distributing around the wheels' circumference at the angle of 45 degree to the wheel plane such that agile mobility in any direction without the change of orientation can be obtained [17,18].

Sliding mode control is known as a variable-structure control method, which generates discontinuous control signals to force the system to 'slide' along a predetermined sliding surface such that the convergence property and control robustness can be achieved [19]. Due to its noteworthy advantages, sliding mode control has been widely utilized in various mechatronic applications such as [20–24]. To enhance the convergence rate and alleviate the chattering phenomenon of conventional sliding mode (CSM) control, a terminal sliding mode (TSM) control method is proposed [25], and gets widely used in numerous applications such as clutch control in automotive transmission systems [26], permanent-magnet synchronous motor control [27] and walker-assisted paraplegic walking control [28]. However, singularity problems are usually found in the design and implementation of TSM control. In order to overcome this shortcoming, a nonsingular terminal sliding mode (NTSM) control scheme is proposed [29]. In [30], an NTSM control strategy combined with an adaptive estimation law is proposed for a vehicle steer-by-wire system, which demonstrates fast convergence property and strong robustness against various road conditions. In [31], a robust NTSM controller is designed for rotor position control of a nonlinear thrust active magnetic bearing system, and achieves finite-time convergence and high tracking precision.

Not restricted in single-input–single-output (SISO) systems, NTSM control also plays an important role in multi–input–multi–output (MIMO) systems such as robot manipulators [32] and six-legged walking robots [33]. In [34], an NTSM control scheme is proposed for three-dimensional motion control of a piezo-flexural nanopositioning stage to achieve robust and accurate trajectory-tracking performance. The remarkable merits of NTSM control including finite-time convergence property and strong robustness against system uncertainties or unmodeled dynamics are pretty beneficial for a mechatronic system like an MWOMR. However, the design and implementation of NTSM control for MWOMRs is still rare, which motivates us to design a robust multi–input–multi–output NTSM controller for the path-following control problem of an MWOMR.

In this paper, a second-order state-space equation with four inputs and three outputs is presented as the plant model to describe the MWOMR's path-following kinematics and dynamics. On the basis of this model, a robust NTSM controller is designed for the MWOMR with rigorous and meticulous stability proof. A Runge–Kutta formula-based dead-reckoning algorithm is proposed to deduce the position and orientation information of the MWOMR. Experiments are carried out to indicate the superior performance of the proposed NTSM control with the assistance of a CSM controller.

The remaining part of this paper is organized as follows. In Section 2, the plant model is identified and elaborated in detail. In Section 3, the NTSM controller is designed for the MWOMR, stability of the control system is verified via Lyapunov, selection guideline of control parameters is described and the dead-reckoning algorithm is presented. In Section 4, experimental results of the NTSM and CSM control are shown, compared and analyzed. Finally, Section 5 concludes this paper.

2. Plant modeling

The top view of an MWOMR is shown in Fig. 1, where $O_qX_qY_q$ is the global coordinate frame; $O_lX_lY_l$ is the coordinate frame located on the MWOMR; O_l represents the geometric center of the robot; and ψ_q denotes the yaw angle of the robot around O_l. Here, we use $P_l = [x_l\ y_l\ \psi_l]^T$ to describe the robot's position in the coordinate of $O_lX_lY_l$, where $[x_l\ y_l]^T$ denotes the position and ψ_l is the orientation. From the view of global coordinate, the MWOMR's position is described by

$$Q = [x_q\ y_q\ \psi_q]^T \tag{1}$$

where $[x_q y_q]^T$ represents the position of the robot's geometric center O_c in the global coordinate $O_qX_qY_q$; ψ_q is the angle between the X_l axis and X_q axis, which can be used to denote the robot's heading direction. Accordingly, the kinematic model of the MWOMR is described as follows [18]:

$$\begin{bmatrix}\dot{x}_l\\ \dot{y}_l\\ \dot{\psi}_l\end{bmatrix} = \frac{r}{4}\begin{bmatrix}-1 & 1 & -1 & 1\\ 1 & 1 & 1 & 1\\ \frac{1}{a+b} & -\frac{1}{a+b} & -\frac{1}{a+b} & \frac{1}{a+b}\end{bmatrix}\cdot\begin{bmatrix}\dot{\theta}_1\\ \dot{\theta}_2\\ \dot{\theta}_3\\ \dot{\theta}_4\end{bmatrix} \tag{2}$$

where r is the radius of Mecanum wheels (four Mecanum wheels are with the same dimension); θ_i is the rotation angle of the i^{th} Mecanum wheel; a and b denote lengths as shown in Fig. 1.

The transforming matrix relating the coordinate systems $O_qX_qY_q$ and $O_lX_lY_l$ is given by [18]:

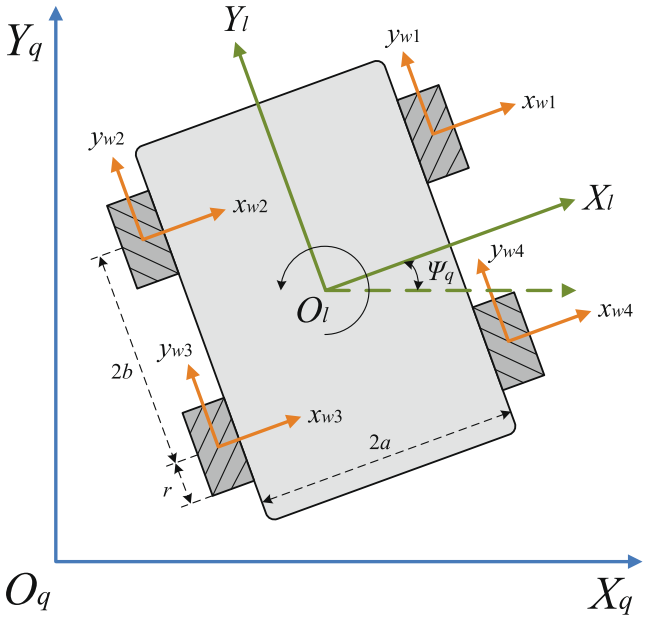

Fig. 1. Top view of MWOMR.

$$R(\psi_q) = \begin{bmatrix} \cos(\psi_q) & -\sin(\psi_q) & 0 \\ \sin(\psi_q) & \cos(\psi_q) & 0 \\ 0 & 0 & 1 \end{bmatrix}. \tag{3}$$

To be more specific, the first-order derivative of the robot's position Q in the $O_qX_qY_q$ coordinate has the following relation with the corresponding one in the $O_lX_lY_l$ coordinate:

$$\begin{bmatrix} \dot{x}_q \\ \dot{y}_q \\ \dot{\psi}_q \end{bmatrix} = R(\psi_q) \begin{bmatrix} \dot{x}_l \\ \dot{y}_l \\ \dot{\psi}_l \end{bmatrix}. \tag{4}$$

Combining (2) and (4), we have

$$\begin{bmatrix} \dot{x}_q \\ \dot{y}_q \\ \dot{\psi}_q \end{bmatrix} = \frac{r}{4} h(\psi)\dot{\theta} \tag{5}$$

where

$$h(\psi) = \begin{bmatrix} -\sqrt{2}\sin(\psi) & \sqrt{2}\cos(\psi) & -\sqrt{2}\sin(\psi) & \sqrt{2}\cos(\psi) \\ \sqrt{2}\cos(\psi) & \sqrt{2}\sin(\psi) & \sqrt{2}\cos(\psi) & \sqrt{2}\sin(\psi) \\ \frac{1}{a+b} & -\frac{1}{a+b} & -\frac{1}{a+b} & \frac{1}{a+b} \end{bmatrix}, \tag{6}$$

$\psi = \psi_q + \frac{\pi}{4}$, and $\theta = [\theta_1 \ \theta_2 \ \theta_3 \ \theta_4]^T$. According to (5), we can get the second-order derivative of Q as

$$\ddot{Q} = \frac{r}{4} h(\psi)'\dot{\theta} + \frac{r}{4} h(\psi)\ddot{\theta} \tag{7}$$

where

$$h(\psi)' = \begin{bmatrix} -\sqrt{2}\cos(\psi) & -\sqrt{2}\sin(\psi) & -\sqrt{2}\cos(\psi) & -\sqrt{2}\sin(\psi) \\ -\sqrt{2}\sin(\psi) & \sqrt{2}\cos(\psi) & -\sqrt{2}\sin(\psi) & \sqrt{2}\cos(\psi) \\ 0 & 0 & 0 & 0 \end{bmatrix}. \tag{8}$$

The dynamic model of the motors associated with the Mecanum wheels can be expressed as follows:

$$J_0\ddot{\theta} + b_0\dot{\theta} + d = v \tag{9}$$

where J_0 is the nominal equivalent moment of inertia of each wheel, b_0 is the nominal viscous friction of each wheel, $d = [d_1, d_2, d_3, d_4]^T$ are the lumped parametric uncertainties of four wheels, and $v = [v_1, v_2, v_3, v_4]^T$ are the input voltages of four corresponding motors. Note that four Mecanum wheels are with the same structure and dimension. Hence, we can assume that J_0 and b_0 are also identical for all the Mecanum wheels.

Our experimental platform of an MWOMR is shown in Fig. 2. From Fig. 2(a) we can see that conventional rubber wheels of a mobile robot have been removed and replaced by four Mecanum wheels. Four DC motors as shown in Fig. 2(b) are controlled to generate appropriate torques to drive the corresponding Mecanum wheels. In the DC motors, encoders are installed to obtain the rotary angles of the corresponding Mecanum wheels. A real-time embedded microcontroller system (NI myRIO) is used to collect encoder measurements and generate control inputs. Two motor drivers are adopted to convert the control input signals to current signals to drive the DC motors.

In our MWOMR, the nominal values of the motor-wheel system are given by

$$\begin{aligned} J_0 &= 0.095\ \text{kgm}^2 \\ b_0 &= 0.087\ \text{Nms/rad}, \end{aligned} \tag{10}$$

and each element of the lumped parametric uncertainties d satisfies the following condition:

$$|d_i| < \bar{d} = 25\ \text{Nm} \tag{11}$$

where $i = 1, 2, 3, 4$ is the index of each Mecanum wheel, and $\bar{d}$ is the upper bound of d_i.

Rearranging (7) yields

$$\ddot{Q} = \frac{r}{4J_0} h(\psi)\left(H\dot{\theta} + J_0\ddot{\theta}\right) \tag{12}$$

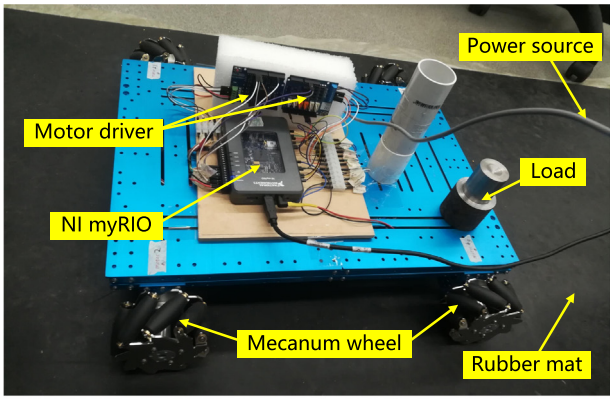

(a)

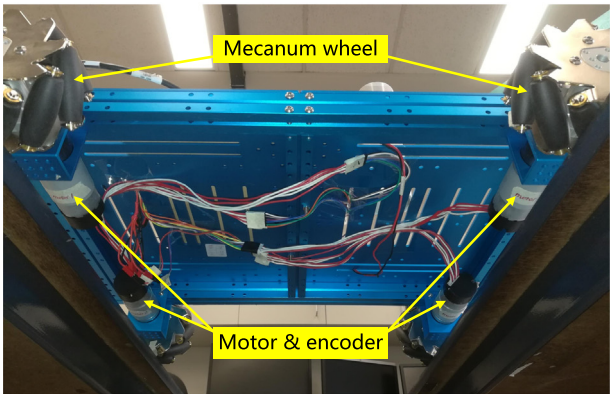

(b)

Fig. 2. Experimental platform of an MWOMR.

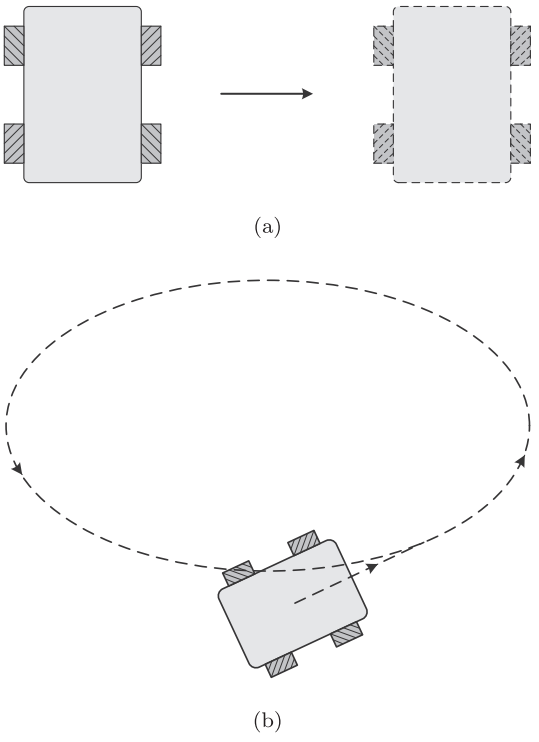

Fig. 3. Schematic of two experimental trajectories. (a) lateral movement, (b) circular movement with initial offset.

where

$$H = \begin{bmatrix} 0 & \frac{J_0}{2} & 0 & \frac{J_0}{2} \\ -\frac{J_0}{2} & 0 & -\frac{J_0}{2} & 0 \\ 0 & \frac{J_0}{2} & 0 & \frac{J_0}{2} \\ -\frac{J_0}{2} & 0 & -\frac{J_0}{2} & 0 \end{bmatrix}. \tag{13}$$

Combining (9) and (12), we obtain

$$\ddot{Q} = \frac{r}{4J_0} h(\psi)\left(H\dot{\theta} - b_0\dot{\theta} - d + v\right). \tag{14}$$

Based on (14), we design the control input v as

$$v = -H\dot{\theta} + b_0\dot{\theta} + u \tag{15}$$

where $u = [u_1\ u_2\ u_3\ u_4]^T$ is the equivalent control input to be designed later. Thus, substituting (15) into (14) yields the equivalent plant model as follows:

$$\ddot{Q} = \frac{r}{4J_0} h(\psi)(u - d). \tag{16}$$

On the basis of the equivalent plant model as shown in (16), it will be more convenient to present the control design of u.

3. Control design

To achieve high path-tracking accuracy and strong robustness against parametric uncertainties and unmodeled dynamics, this section presents the design of NTSM controller based on the equivalent plant model given by (16).

3.1. NTSM controller

Let the tracking error e be

$$e = \begin{bmatrix} e_1 \\ e_2 \\ e_3 \end{bmatrix} = \begin{bmatrix} x_q - x_r \\ y_q - y_r \\ \psi_q - \psi_r \end{bmatrix} \tag{17}$$

where $Q_r = [x_r \ y_r \ \psi_r]^T$ is the reference signal of the control system.

Then, we define the sliding variable s as

$$s = \begin{bmatrix} s_1 \\ s_2 \\ s_3 \end{bmatrix} = \begin{bmatrix} e_1 + \lambda_1(\dot{e}_1)^{p/q} \\ e_2 + \lambda_2(\dot{e}_2)^{p/q} \\ e_3 + \lambda_3(\dot{e}_3)^{p/q} \end{bmatrix} \tag{18}$$

where $p > 0, q > 0$ are odd integers to be designed to satisfy $1 < \frac{p}{q} < 2$, and $\lambda_1 > 0, \lambda_2 > 0, \lambda_3 > 0$ are control parameters to be designed. Rearranging (18) yields

$$s = e + \lambda(\dot{e})^{\frac{p}{q}} \tag{19}$$

where

$$\lambda = \begin{bmatrix} \lambda_1 & 0 & 0 \\ 0 & \lambda_2 & 0 \\ 0 & 0 & \lambda_3 \end{bmatrix}. \tag{20}$$

Based on (19), taking the first-order derivative of the sliding variable s yields

$$\dot{s} = \dot{e} + M\ddot{e} \tag{21}$$

where

$$M = \begin{bmatrix} \frac{\lambda_1 p}{q}(\dot{e}_1)^{\frac{p}{q}-1} & 0 & 0 \\ 0 & \frac{\lambda_2 p}{q}(\dot{e}_2)^{\frac{p}{q}-1} & 0 \\ 0 & 0 & \frac{\lambda_3 p}{q}(\dot{e}_3)^{\frac{p}{q}-1} \end{bmatrix}. \tag{22}$$

Based on the definition of equivalent control input elaborated in [19], if we neglect the lumped parametric uncertainties and unmodeled dynamics, namely, suppose $d = [d_1 \ d_2 \ d_3 \ d_4]^T = [0 \ 0 \ 0 \ 0]^T$, and solve the sliding mode dynamics given by

$$\dot{s} = \dot{e} + M\ddot{e} = \dot{e} + M\left(\ddot{Q} - \ddot{Q}_r\right) = 0, \tag{23}$$

then we can obtain an equivalent control input u_{eq} as follows:

$$u_{eq} = \frac{4J_0}{r} h(\psi)^{-1}\left[\ddot{Q}_r - M^{-1}\dot{e}\right] \tag{24}$$

where

$$h(\psi)^{-1} = \frac{1}{4}\begin{bmatrix} -\sqrt{2}\sin(\psi) & \sqrt{2}\cos(\psi) & a+b \\ \sqrt{2}\cos(\psi) & \sqrt{2}\sin(\psi) & -(a+b) \\ -\sqrt{2}\sin(\psi) & \sqrt{2}\cos(\psi) & -(a+b) \\ \sqrt{2}\cos(\psi) & \sqrt{2}\sin(\psi) & a+b \end{bmatrix} \tag{25}$$

and

$$M^{-1} = \begin{bmatrix} \frac{q}{p\lambda_1}(\dot{e}_1)^{1-\frac{p}{q}} & 0 & 0 \\ 0 & \frac{q}{p\lambda_2}(\dot{e}_2)^{1-\frac{p}{q}} & 0 \\ 0 & 0 & \frac{q}{p\lambda_3}(\dot{e}_3)^{1-\frac{p}{q}} \end{bmatrix}. \tag{26}$$

To guarantee the control robustness against the lumped parametric uncertainties and unmodeled dynamics existing in the system, a reaching control input u_r [19] is designed as:

$$u_r = -h(\psi)^{-1} \cdot B \cdot \mathrm{sign}(s). \tag{27}$$

In (27), $h(\psi)^{-1}$ and s are given by (25) and (19), and B is designed as

$$B = \begin{bmatrix} 8\bar{d} \\ 8\bar{d} \\ \frac{4\bar{d}}{a+b} \end{bmatrix} \tag{28}$$

where $\bar{d}$ is given by (11).

Lemma 1. For the MWOMR path-following control system (12) with the lumped parametric uncertainties and unmodeled dynamics d in (9), the control input is designed as follows:

$$\begin{aligned} v = & -\begin{bmatrix} 0 & \frac{J_0}{2} & 0 & \frac{J_0}{2} \\ -\frac{J_0}{2} & 0 & -\frac{J_0}{2} & 0 \\ 0 & \frac{J_0}{2} & 0 & \frac{J_0}{2} \\ -\frac{J_0}{2} & 0 & -\frac{J_0}{2} & 0 \end{bmatrix} \dot{\theta} + b_0\dot{\theta} + u \\ u = & \ u_{eq} + u_r \end{aligned} \tag{29}$$

where u_{eq} and u_r are given by (24) and (27), respectively. Then, the tracking error e defined in (17) can converge to zero for a given reference path.

Proof: A Lyapunov function V is chosen as

$$V = \frac{1}{2}s^T s. \tag{30}$$

Taking the first-order derivative of the Lyapunov function V yields

$$\begin{aligned} \dot{V} = & \ s_1\dot{s}_1 + s_2\dot{s}_2 + s_3\dot{s}_3 \\ = & \ s^T\dot{s}. \end{aligned} \tag{31}$$

We take the first-order derivative of the sliding variable s and obtain

$$\dot{s} = \dot{e} + M\ddot{Q} - M\ddot{Q}_r.$$

Substituting (16) into (32) yields

$$\dot{s} = \dot{e} - M\ddot{Q}_r + M\left[\frac{r}{4J_0}h(\psi)(u-d)\right] = \dot{e} - M\ddot{Q}_r - \frac{r}{4J_0}Mh(\psi)d + \frac{r}{4J_0}Mh(\psi)u. \tag{33}$$

Then we substitute the control input u defined in (29) into (33) and obtain

$$\begin{aligned} \dot{s} = & \dot{e} - M\ddot{Q}_r + M\left[\frac{r}{4J_0}h(\psi)(u-d)\right] \\ = & \dot{e} - M\ddot{Q}_r - \frac{r}{4J_0}Mh(\psi)d + \frac{r}{4J_0}Mh(\psi)u \\ = & \dot{e} - M\ddot{Q}_r - \frac{r}{4J_0}Mh(\psi)d + \frac{r}{4J_0}Mh(\psi)\cdot\left[\frac{4J_0}{r}h(\psi)^{-1}\left(\ddot{Q}_r - M^{-1}\dot{e}\right) - h(\psi)^{-1}B\mathrm{sign}(s)\right] \\ = & -\frac{r}{4J_0}Mh(\psi)d - \frac{r}{4J_0}MB\mathrm{sign}(s) \\ = & \frac{r}{4J_0}M[-h(\psi)d - B\mathrm{sign}(s)]. \end{aligned} \tag{34}$$

Substituting (34) into (31) yields

$$\dot{V} = \frac{r}{4J_0}s^T M[-h(\psi)d - B\mathrm{sign}(s)] = \frac{r}{4J_0}\left[M_1(A_1s_1 - 8\bar{d}|s_1|) + M_2(A_2s_2 - 8\bar{d}|s_2|) + M_3\left(A_3s_3 - \frac{4\bar{d}}{a+b}|s_3|\right)\right] \tag{35}$$

where

$$\begin{cases} M_1 = \frac{\lambda_1 p}{q}(\dot{e}_1)^{p/q-1} \\ M_2 = \frac{\lambda_2 p}{q}(\dot{e}_2)^{p/q-1} \\ M_3 = \frac{\lambda_3 p}{q}(\dot{e}_3)^{p/q-1} \end{cases} \tag{36}$$

and

$$\begin{cases} A_1 = \sqrt{2}\sin(\psi)d_1 - \sqrt{2}\cos(\psi)d_2 + \sqrt{2}\sin(\psi)d_3 - \sqrt{2}\cos(\psi)d_4 \\ A_2 = -\sqrt{2}\cos(\psi)d_1 - \sqrt{2}\sin(\psi)d_2 - \sqrt{2}\cos(\psi)d_3 - \sqrt{2}\sin(\psi)d_4 \\ A_3 = -\frac{1}{a+b}d_1 + \frac{1}{a+b}d_2 + \frac{1}{a+b}d_3 - \frac{1}{a+b}d_4. \end{cases} \tag{37}$$

In (36), $\lambda_1 > 0, \lambda_2 > 0, \lambda_3 > 0$ are control parameters to be designed; $p > 0, q > 0$ must be selected as odd integers satisfying the condition of $1 < \frac{p}{q} < 2$. Thus, the following inequations establish:

$$M_1 \geq 0,\ M_2 \geq 0,\ M_3 \geq 0. \tag{38}$$

Based on (11) and the expression of A_1, A_2 and A_3 given by (37), we can conclude that

$$\begin{cases} A_1 < 8\bar{d} \\ A_2 < 8\bar{d} \\ A_3 < \frac{4\bar{d}}{a+b}, \end{cases} \tag{39}$$

and further deduce that

$$\begin{cases} A_1 s_1 < 8\bar{d}|s_1| \\ A_2 s_2 < 8\bar{d}|s_2| \\ A_3 s_3 < \frac{4\bar{d}}{a+b}|s_3| \end{cases} \tag{40}$$

when $s \neq 0$. Finally, according to (35), (38) and (40), we can conclude that

$$\dot{V} < 0 \tag{41}$$

when $s \neq 0$. Hence, it is theoretically proved that $s_1 \to 0, s_2 \to 0$ and $s_3 \to 0$, where the symbol '$\to$' is used to represent 'converges to'. Based on the definition of s_1, s_2 and s_3 given by (18), it can be concluded that $e_1 \to 0, e_2 \to 0$ and $e_3 \to 0$ [29], namely,

$$\begin{aligned} x_q &\to x_r \\ y_q &\to y_r \\ \psi_q &\to \psi_r. \end{aligned} \tag{42}$$

Thus, the proof is completed.

3.2. Selection of control parameters

Up to now, we have designed the NTSM controller for the MWOMR and proved the stability of the closed-loop control system in the sense of Lyapunov. However, whether the proposed NTSM control scheme can achieve satisfactory path-following performance also depends on appropriate selection of control parameters.

Selection of λ_i: From (19) we can see that the parameter $\lambda_i > 0$ primarily determines the bandwidth of the sliding mode dynamics and the decaying rate of the tracking errors [30,30]. Specifically, setting a smaller λ_i can lead to a larger sliding mode bandwidth, which implies higher tracking accuracy. However, decreasing the value of λ_i beyond a certain level will introduce extra measurement noises and amplify the chattering phenomenon. Considering the tradeoff between the control precision and smoothness, we set $\lambda_1 = \lambda_2 = \lambda_2 = 1.5$.

Selection of p and q: According to [29], the parameters p and q must be chosen as positive odd integers satisfying $1 < \frac{p}{q} < 2$ such that the singularity problem existing in TSM control can be solved. Theoretically, increasing the value of $\frac{p}{q}$ leads to a faster convergence rate of tracking errors but at the cost of causing severer chattering in the input voltages of DC motors. In experiments, we find that the setting of $p = 5$ and $q = 3$ can strike a good balance between the convergence rate and chattering suppression.

3.3. CSM control for comparison

In order to test and demonstrate the superiority of the proposed NTSM control scheme, a CSM controller is also designed for the MWOMR on the basis of [19]. For simplicity, the stability proof is omitted and the CSM control input u_{csm} is straightforwardly given here:

$$u_{csm} = h(\psi)^{-1}\left[\frac{4J_0}{r}\left(\ddot{Q}_r + \lambda_c \dot{e}_c\right) + N\mathrm{sign}(s_c)\right] \tag{43}$$

where e_c is the tracking error of the CSM control system with the definition of

$$e_c = \begin{bmatrix} e_{c1} \\ e_{c2} \\ e_{c3} \end{bmatrix} = \begin{bmatrix} x_r - x_q \\ y_r - y_q \\ \psi_r - \psi_q \end{bmatrix}, \tag{44}$$

and s_c is a CSM variable defined as

$$s_c = \dot{e}_c + \lambda_c e_c. \tag{45}$$

In (43), λ_c is the bandwidth of the sliding mode surface s_c, whose value is set as

$$\lambda_c = \begin{bmatrix} 8 & 0 & 0 \\ 0 & 8 & 0 \\ 0 & 0 & 8 \end{bmatrix}, \tag{46}$$

and N is the switching function gain with the value shown as follows:

$$N = \begin{bmatrix} 8\bar{d} \\ 8\bar{d} \\ \frac{4\bar{d}}{a+b} \end{bmatrix} \tag{47}$$

where $\bar{d}$ is the upper bound of the parametric uncertainties d_i given by (11).

3.4. Dead reckoning

The aim of the dead-reckoning scheme is to numerically calculate a moving object's position and pose in the global coordinate framework on the basis of an accurate initial position. For our MWOMR path-tracking control system, an available dead-reckoning approach is required to deduce the robot's position and yaw angle by means of the kinematic model expressed in (5) and (6), the velocity information from wheel motor encoders and an effective numerical algorithm. Researchers have employed various numerical algorithms to solve dead-reckoning problems, such as the Runge–Kutta method and the Euler formula. Considering the tradeoff between design simplicity and calculation accuracy, we adopt the following dead-reckoning algorithm based on a second-order Runge–Kutta formula [35]:

$$\begin{bmatrix} x_q(k) \\ y_q(k) \\ \psi_q(k) \end{bmatrix} = \begin{bmatrix} x_q(k-1) \\ y_q(k-1) \\ \psi_q(k-1) \end{bmatrix} + \frac{r}{4} \cdot \frac{T\left[h(\psi(k-1))\dot{\theta}(k-1) + h(\psi(k))\dot{\theta}(k)\right]}{2} \tag{48}$$

where T is the sampling period that is set as sufficiently small; $*(k)$ denotes the current status of the parameter $*$ at the k^{th} sampling instant, and $*(k-1)$ denotes the previous status of the parameter $*$ at the $(k-1)^{\text{th}}$ sampling instant.

4. Experimental results

Experiments are carried out through our MWOMR experimental setup as shown in Fig. 2 to test the performance of designed controllers. To demonstrate the advantages of the Mecanum-wheel mechanism and make a fair comparison between the NTSM control and CSM control, two cases of lateral movement and circular movement with initial offset are arranged in experiments, whose basic explanatory schematics are shown in Fig. 3(a) and (b), respectively.

4.1. Case 1: lateral movement

For a normal rubber-wheels mobile robot, a sharp change of moving direction must be executed by differential steering, which requires a larger space compared with an MWOMR. The capability of flexible switching from longitudinal movement to lateral movement gives the MWOMR irreplaceable benefits for working in narrow places. In this case, the MWOMR is controlled to move along the X-axis in two trials, in which the control input signals are managed by the NTSM controller and the CSM controller, respectively. The duration of the experiment is set as 9 s, and the reference linear speed for the MWOMR is 0.25 m/s.

The experimental results of the NTSM and CSM control in this case are shown in Figs. 4–6. From Fig. 4, we can see that the tracking performance of the NTSM control is superior to that of the CSM control generally, which is reflected in smaller amplitudes of the oscillations along the reference Y-axis displacement and orientation angle. Fig. 5 shows the tracking errors under these two control schemes. It is seen that the steady-state X-axis error under the CSM control is about 44 mm. However, this error under the NTSM control is 20 mm, which is obviously smaller. From Fig. 5(b) we can see that the peak Y-axis error under the NTSM control is about 8 mm, which is bigger than that of the CSM control. Nevertheless, this peak value appears at the very beginning of the experiment. After the Y-axis errors converge to steady state, the amplitude of Y-axis

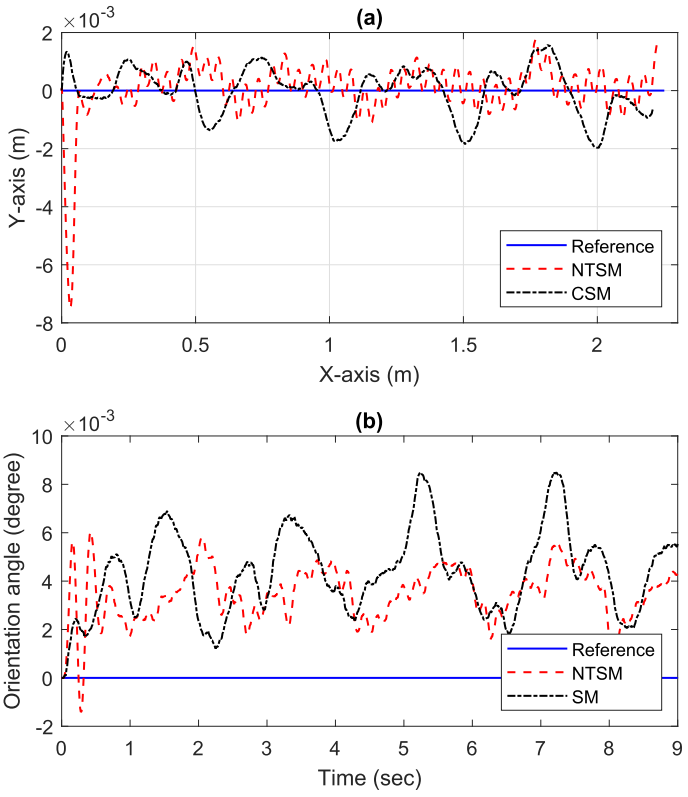

Fig. 4. Tracking profiles in Case 1. (a) Comparison of trajectories, (b) Comparison of orientation angles.

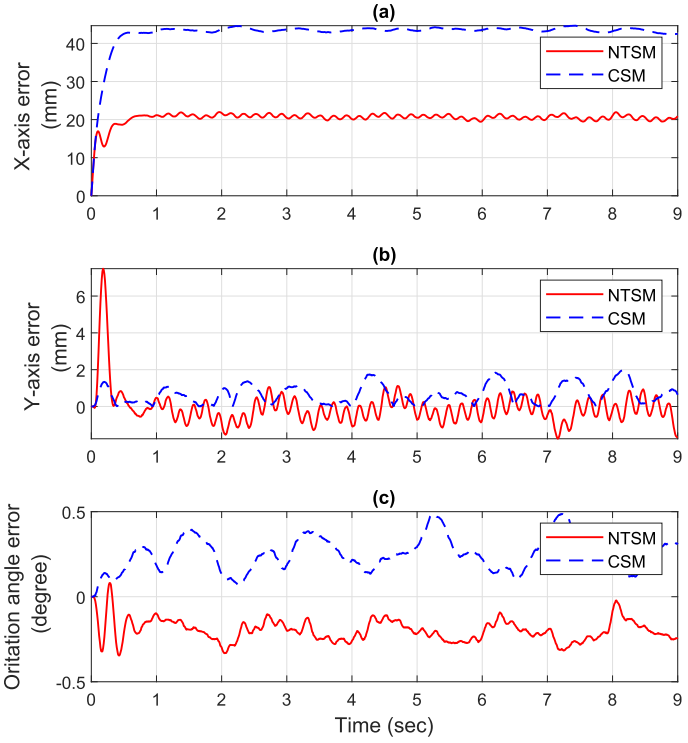

Fig. 5. Tracking errors in Case 1. (a) Tracking errors of X-axis displacement, (b) Tracking errors of Y-axis displacement, (c) Tracking errors of orientation angle.

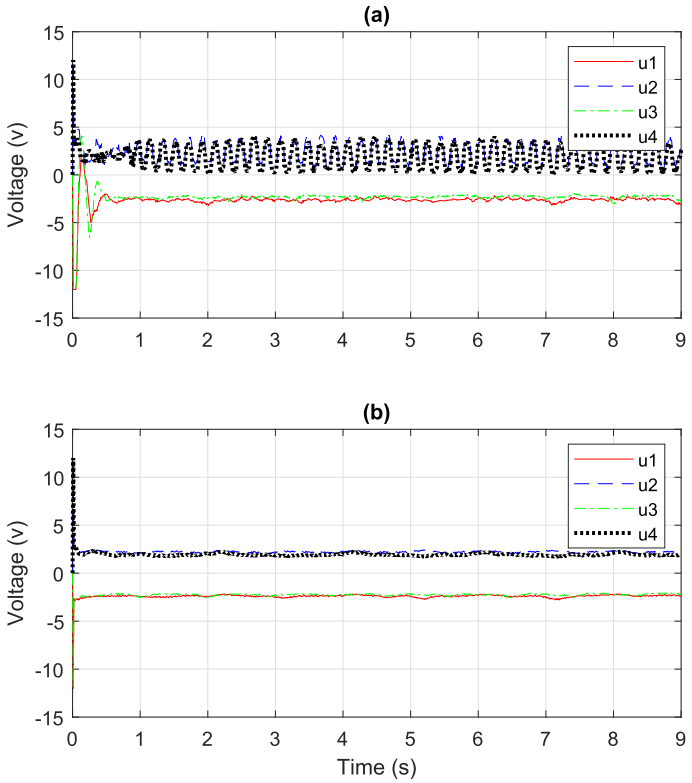

Fig. 6. Control inputs in Case 1. (a) Control inputs of NTSM, (b) Control inputs of CSM.

error under the NTSM control is smaller than that of the CSM control at most time. The peak orientation-angle error under the CSM control is 0.5 degree, while the corresponding one of the NTSM control is about −0.3 degree. Furthermore, the steady-state orientation-angle error under the NTSM control is evidently smaller than that of the CSM control. Therefore, it can be concluded that the tracking precision of the NTSM control is higher in comparison with the CSM control. We must admit that the NTSM control input signals contain more chattering than those of the CSM controller as shown in Fig. 6. However, considering the superior performance of the NTSM control, this small cost is regarded as totally worthy.

4.2. Case 2: circular movement with offset

In Case 1, we have tested the lateral-movement performance of our MWOMR under the NTSM and CSM control, which strongly proves the benefits of the Mecanum-wheel mechanism and the NTSM control scheme. In reality, the working performance of a mobile robot in a larger space is also of great importance due to the dimensions of factories and warehouses. Circular path is simple and popular in testing the path-following performance of a mobile robot. In this case, the MWOMR is supposed to move along a circle with a linear speed of 0.42 m/s. Besides, to test the adaptivity of the control system, the starting point is not the origin (0, 0), but is with an offset and located at (0.1, 0.1). Thus, the MWOMR is required to approach the trajectory linearly before it begins a circular movement.

The experimental results in Case 2 are shown in Figs. 7–9, which are the tracking profiles, tracking errors and control inputs, respectively. From Fig. 7, we can see that both the NTSM and CSM controllers can force the MWOMR to finish the circular path-following task with linear increasing orientation angles. The superiority of the NTSM control is mainly reflected by Fig. 8. In Fig. 8(a), it is shown that the peak X-axis errors of both controllers are nearly the same. However, the steady-state X-axis error under the NTSM control is evidently smaller than that of the CSM control. Similar situation also happens for the Y-axis errors as shown in Fig. 8(b). From Fig. 8(c) we can see that the peak orientation error under the CSM control is about 9 degree. Nevertheless, the corresponding one of the NTSM control is only 7 degree. In addition, the steady-state orientation angle error under the CSM control is approximately 4 degree, which is much larger than that of the NTSM control with the value of only 2 degree. Therefore, we can conclude that the tracking precision of the NTSM control is still higher in Case 2 compared with the CSM control. Similar to the situation in Case 1, the control inputs of the NTSM controller perform severer chattering than those of the CSM controller, which is exhibited in Fig. 9. However, taking consideration of the superior circular path-following performance of the NTSM control scheme, we think that this sacrifice in control smoothness is acceptable, especially the oscillation in the tracking profiles as shown in Fig. 7 is pretty inconspicuous.

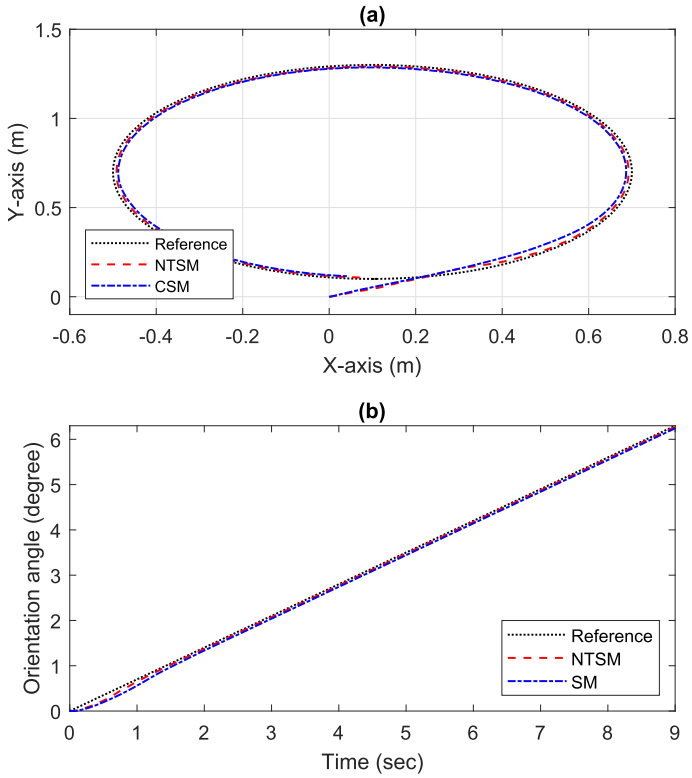

Fig. 7. Tracking profiles in Case 2. (a) Comparison of trajectories, (b) Comparison of orientation angles.

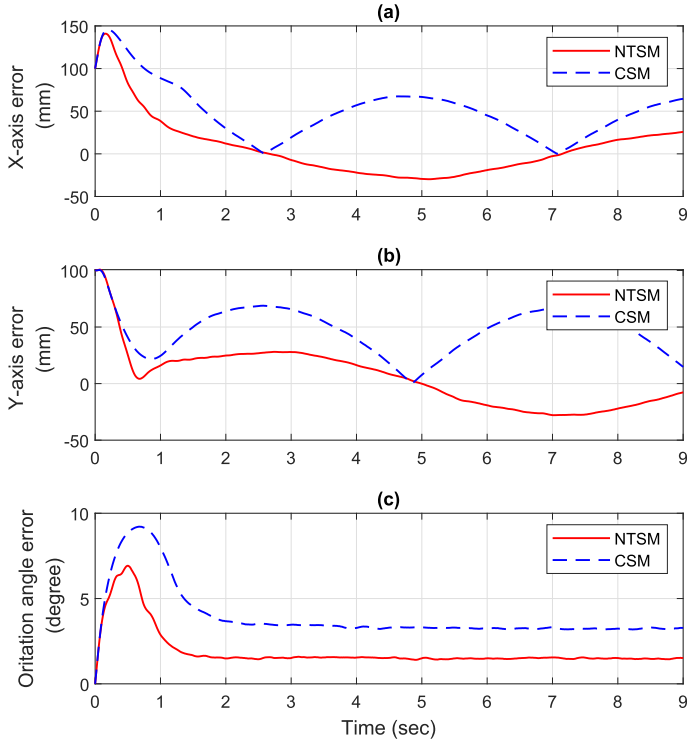

Fig. 8. Tracking errors in Case 2. (a) Tracking errors of X-axis displacement, (b) Tracking errors of Y-axis displacement, (c) Tracking errors of orientation angle.

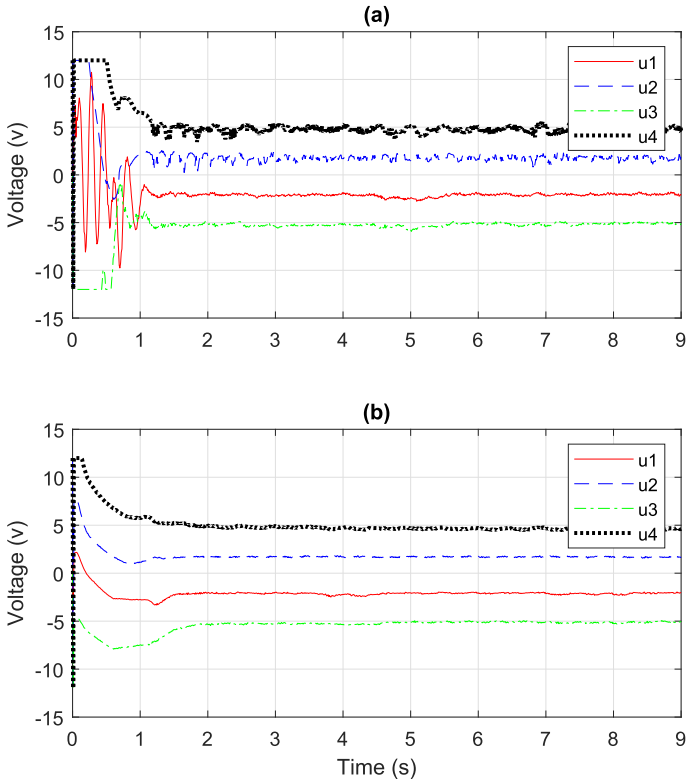

Fig. 9. Control inputs in Case 2. (a) Control inputs of NTSM, (b) Control inputs of CSM.

5. Conclusion

In this paper, an NTSM control scheme is proposed for an MWOMR to achieve satisfactory path-tracking performance. The stability of the NTSM control system is theoretically proved in the sense of Lyapunov. In addition, the guideline for setting proper values of the NTSM control parameters is elaborated in detail, which reasonably compromises the desired tracking performance with sensor measurement noises and system uncertainties. A Runge–Kutta formula-based dead reckoning algorithm is employed to calculate the position and angle information in real time. Finally, experimental results in both the scenarios of lateral movement and circular movement are shown. It is demonstrated that the presented NTSM control strategy possesses remarkable benefits reflected in higher tracking precision and stronger robustness in comparison with the CSM control. Definitely, the superior tracking performance of the NTSM controller is at the cost of a larger computational load on the control system hardware. Nevertheless, the fast updating speed of the processor and embedded system technology will make this issue trivial.

Currently, restricted by the experimental platform, the position-detection scheme for our MWOMR is by utilizing the dead-reckoning approach. However, with the existing of slip between the Mecanum wheels and the rubber mat, the position errors will accumulate and the theoretical position will deviate from the actual one further and further. Hence, our future work is to enhance the experimental setup by means of introducing sensing devices such as ultrasonic sensors and active beacon's transmitters. Then, the design and implementation of robust control algorithms in MWOMR can be accomplished in a more convincing way. In addition, the proposed NTSM control scheme enhances the tracking precision but at the cost of triggering more chattering compared with the CSM control. Though this cost is considered to be worthy to a large extent, the chattering is still an issue worth solving in the future. Our next plan is to investigate chattering-free control strategies for MWOMRs such that the tracking performance could be further improved.

CRediT authorship contribution statement

Zhe Sun: Writing - original draft. **Hao Xie**: Data curation. **Jinchuan Zheng**: Supervision. **Zhihong Man**: Conceptualization. **Defeng He**: Resources.

Declaration of Competing Interest

The authors declare that they have no known competing financial interests or personal relationships that could have appeared to influence the work reported in this paper.

References

[1] A. Odry, R. Fuller, I.J. Rudas, P. Odry, Kalman filter for mobile-robot attitude estimation: novel optimized and adaptive solutions, Mech. Syst. Signal Process. 110 (2018) 569–589.
[2] Y. Kantaros, M.M. Zavlanos, Distributed intermittent connectivity control of mobile robot networks, IEEE Trans. Autom. Control 62 (7) (2017) 3109–3121.
[3] K.J. Kalinski, M. Mazur, Optimal control of 2-wheeled mobile robot at energy performance index, Mech. Syst. Signal Process. 70 (2016) 373–386.
[4] S. Zhao, B. Huang, F. Liu, Localization of indoor mobile robot using minimum variance unbiased FIR filter, IEEE Trans. Autom. Sci. Eng. 15 (2) (2018) 410–419.
[5] P. Kassaeiyan, B. Tarvirdizadeh, K. Alipour, Control of tractor-trailer wheeled robots considering self-collision effect and actuator saturation limitations, Mech. Syst. Signal Process. 127 (2019) 388–411.
[6] P. Panahandeh, K. Alipour, B. Tarvirdizadeh, A. Hadi, A kinematic Lyapunov-based controller to posture stabilization of wheeled mobile robots, Mech. Syst. Signal Process., 134, 2019, Article 106319.
[7] J.J. Craig, Introduction to Robotics: Mechanics and Control, Pearson Education Inc, 1995.
[8] H. Sira-Ramirez, C. Lopez-Uribe, M. Velasco-Villa, Linear observer-based active disturbance rejection control of the omnidirectional mobile robot, Asian J. Control 15 (1) (2013) 51–63.
[9] R. Chao, S. Ma, Generalized proportional integral observer based control of an omnidirectional mobile robot, Mechatronics 26 (2015) 36–44.
[10] M. Wada, H. Asada, Design and control of a variable footprint mechanism for holonomic omnidirectional vehicles and its application to wheelchairs, IEEE Trans. Rob. Autom. 15 (6) (1999) 978–989.
[11] S. Ostrovskaya, R.J. Spiteri, J. Angeles, Dynamics of a mobile robot with three ball-wheels, Int. J. Robot. Res. 19 (4) (2000) 383–393.
[12] W. Chen, C. Chen, J. Tsai, J. Yang, P. Lin, Design and implementation of a ball-driven omnidirectional spherical robot, Mech. Mach. Theory 68 (2013) 35–48.
[13] J.C.L. Barreto, A.G.S. Conceicao, C.E.T. Dorea, L. Martinez, E.R. Pieri, Design and implementation of model-predictive control with friction compensation on an omnidirectional mobile robot, IEEE/ASME Trans. Mechatron. 19 (2) (2014) 467–476.
[14] D. Zhao, X. Deng, J. Yi, Motion and internal force control for omnidirectional wheeled mobile robot, IEEE/ASME Trans. Mechatron. 14 (3) (2009) 382–387.
[15] H. Fukushima, S. Satomura, T. Kawai, M. Tanaka, T. Kamegawa, F. Matsuno, Modeling and control of a snake-like robot using the screw-drive mechanism, IEEE Trans. Rob. 28 (3) (2012) 541–554.
[16] T. Terakawa, M. Komori, K. Matsuda, S. Mikami, A novel omnidirectional mobile robot with wheels connected by passive sliding joints, IEEE/ASME Trans. Mechatron. 23 (4) (2018) 1716–1727.
[17] L.-C. Lin, H.-Y. Shih, Modeling and adaptive control of an omni-Mecanum-wheeled robot, Intell. Control Autom. 4 (2013) 166–179.
[18] J.A. Cooney, W.L. Xu, G. Bright, Visual dead-reckoning for motion contol of a Mecanum-wheeled mobile robot, Mechatronics 14 (2004) 623–637.
[19] J.E. Slotine, W. Li, Applied Nonlinear Control, Prentice-Hall, Englewood Cliffs, NJ, USA, 1991.
[20] I.F. Jasim, P.W. Plapper, H. Voos, Adaptive sliding mode fuzzy control for unknown robots with arbitrarily-switched constraints, Mechatronics 30 (2015) 174–186.
[21] Z. Sun, J. Zheng, Z. Man, H. Wang, Robust control of a vehicle steer-by-wire system using adaptive sliding mode, IEEE Trans. Industr. Electron. 63 (4) (2016) 2251–2262.
[22] S.Y. Chen, S.S. Gong, Speed tracking control of pneumatic motor servo systems using observation-based adaptive dynamic sliding-mode control, Mech. Syst. Signal Process. 94 (15) (2017) 111–128.
[23] L.A. Tuan, S.-G. Lee, Modeling and advanced sliding mode controls of crawler cranes considering wire rope elasticity and complicated operations, Mech. Syst. Signal Process. 103 (15) (2018) 250–263.
[24] S. Wan, X. li, W. Sun, J. Yuan, J. Hong, Active chatter suppression for milling process with sliding mode control and electromagnetic actuator, Mech. Syst. Signal Process., 136, 2020, Article 106528.
[25] Z. Man, A.P. Paplinski, H.R. Wu, A robust MIMO terminal sliding mode control scheme for rigid robotic manipulators, IEEE Trans. Autom. Control 39 (12) (1994) 2464–2469.
[26] S. Li, C. Wu, Z. Sun, Design and implementation of clutch control for automotive transmissions using terminal-sliding-mode control and uncertainty observer, IEEE Trans. Veh. Technol. 65 (4) (2016) 1890–1898.
[27] Y. Feng, J. Zheng, X. Yu, N.V. Truong, Hybrid terminal sliding-mode observer design method for a permanent-magnet synchronous motor control system, IEEE Trans. Industr. Electron. 56 (9) (2009) 3424–3431.
[28] V. Nekoukar, A. Erfanian, A decentralized modular control framework for robust control of FES-activated walker-assisted paraplegic walking using terminal sliding mode and fuzzy logic control, IEEE Trans. Biomed. Eng. 59 (10) (2012) 2818–2827.
[29] Y. Feng, X. Yu, Z. Man, Non-singular terminal sliding mode control of rigid manipulators, Automatica 38 (12) (2002) 2159–2167.
[30] Z. Sun, J. Zheng, H. Wang, Z. Man, Adaptive fast non-singular terminal sliding mode control for a vehicle steer-by-wire system, IET Control Theory Appl. 11 (8) (2017) 1245–1254.
[31] S.-Y. Chen, F.-J. Lin, Robust nonsingular terminal sliding-mode control for nonlinear magnetic bearing system, IEEE Trans. Control Syst. Technol. 19 (3) (2011) 636–643.
[32] M. Jin, J. Lee, P.H. Chang, C. Choi, Practical nonsingular terminal sliding-mode control of robot manipulators for high-accuracy tracking control, IEEE Trans. Industr. Electron. 56 (9) (2009) 3593–3601.
[33] G. Chen, B. Jin, Y. Chen, Nonsingular fast terminal sliding mode posture control for six-legged walking robots with redundant actuation, Mechatronics 50 (2018) 1–15.
[34] F.-J. Lin, S.-Y. Lee, P.-H. Chou, Intelligent nonsingular terminal sliding-mode control using MIMO Elman neural network for piezo-flexural nanopositioning stage, IEEE Trans. Ultrason. Ferroelectr. Freq. Control 59 (12) (2012) 2716–2730.
[35] C.-C. Tsai, F.-C. Tai, Y.-C. Wang, Global localization using dead-reckoning and kinect sensors for robots with omnidirectional mecanum wheels, J. Mar. Sci. Technol. 22 (3) (2014) 321–330.